DESY 99-094
July 1999

ISSN 0418-9833

Forward π°-Meson Production at HERA

H1 Collaboration

Abstract

High transverse momentum π°-mesons have been measured with the H1 detector at HERA in deep-inelastic ep scattering events at low Bjorken-x, down to $x \approx 4{\cdot}10^{-5}$. The measurement is performed in a region of small angles with respect to the proton remnant in the laboratory frame of reference, namely the forward region, and corresponds to central rapidity in the centre of mass system of the virtual photon and proton. This region is expected to be particularly sensitive to QCD effects in hadronic final states. Differential cross-sections for inclusive π°-meson production are presented as a function of Bjorken-x and the four-momentum transfer Q^2, and as a function of transverse momentum and pseudorapidity. A recent numerical BFKL calculation and predictions from QCD models based on DGLAP parton evolution are compared with the data.

To be submitted to Phys. Lett.

H1 Collaboration

C. Adloff[33], V. Andreev[24], B. Andrieu[27], V. Arkadov[34], A. Astvatsatourov[34], I. Ayyaz[28], A. Babaev[23], J. Bähr[34], P. Baranov[24], E. Barrelet[28], W. Bartel[10], U. Bassler[28], P. Bate[21], A. Beglarian[10,39], O. Behnke[10], C. Beier[14], A. Belousov[24], T. Benisch[10], Ch. Berger[1], G. Bernardi[28], T. Berndt[14], G. Bertrand-Coremans[4], P. Biddulph[21], J.C. Bizot[26], K. Borras[7], V. Boudry[27], W. Braunschweig[1], V. Brisson[26], H.-B. Bröker[2], D.P. Brown[21], W. Brückner[12], P. Bruel[27], D. Bruncko[16], J. Bürger[10], F.W. Büsser[11], A. Bunyatyan[12,39], S. Burke[17], A. Burrage[18], G. Buschhorn[25], A.J. Campbell[10], J. Cao[26], T. Carli[25], E. Chabert[22], M. Charlet[4], D. Clarke[5], B. Clerbaux[4], C. Collard[4], J.G. Contreras[8,43], J.A. Coughlan[5], M.-C. Cousinou[22], B.E. Cox[21], G. Cozzika[9], J. Cvach[29], J.B. Dainton[18], W.D. Dau[15], K. Daum[33,38], M. David[9,†] M. Davidsson[20], B. Delcourt[26], R. Demirchyan[10,39], A. De Roeck[10], E.A. De Wolf[4], C. Diaconu[22], P. Dixon[19], V. Dodonov[12], K.T. Donovan[19], J.D. Dowell[3], A. Droutskoi[23], C. Duprel[2], J. Ebert[33], G. Eckerlin[10], D. Eckstein[34], V. Efremenko[23], S. Egli[36], R. Eichler[35], F. Eisele[13], E. Eisenhandler[19], E. Elsen[10], M. Erdmann[10,40,f], A.B. Fahr[11], P.J.W. Faulkner[3], L. Favart[4], A. Fedotov[23], R. Felst[10], J. Feltesse[9], J. Ferencei[10], F. Ferrarotto[31], S. Ferron[27], M. Fleischer[10], G. Flügge[2], A. Fomenko[24], I. Foresti[36], J. Formánek[30], J.M. Foster[21], G. Franke[10], E. Gabathuler[18], K. Gabathuler[32], J. Garvey[3], J. Gassner[32], J. Gayler[10], R. Gerhards[10], S. Ghazaryan[10,39], A. Glazov[34], L. Goerlich[6], N. Gogitidze[24], M. Goldberg[28], I. Gorelov[23], C. Grab[35], H. Grässler[2], T. Greenshaw[18], R.K. Griffiths[19], G. Grindhammer[25], T. Hadig[1], D. Haidt[10], L. Hajduk[6], V. Haustein[33], W.J. Haynes[5], B. Heinemann[10], G. Heinzelmann[11], R.C.W. Henderson[17], S. Hengstmann[36], H. Henschel[34], R. Heremans[4], G. Herrera[7,41,l], I. Herynek[29], M. Hilgers[35], K.H. Hiller[34], C.D. Hilton[21], J. Hladký[29], P. Höting[2], D. Hoffmann[10], R. Horisberger[32], S. Hurling[10], M. Ibbotson[21], Ç. İşsever[7], M. Jacquet[26], M. Jaffre[26], L. Janauschek[25], D.M. Jansen[12], X. Janssen[4], L. Jönsson[20], D.P. Johnson[4], M. Jones[18], H. Jung[20], H.K. Kästli[35], D. Kant[19], M. Kapichine[8], M. Karlsson[20], O. Karschnick[11], O. Kaufmann[13], M. Kausch[10], F. Keil[14], N. Keller[13], I.R. Kenyon[3], S. Kermiche[22], C. Kiesling[25], M. Klein[34], C. Kleinwort[10], G. Knies[10], H. Kolanoski[37], S.D. Kolya[21], V. Korbel[10], P. Kostka[34], S.K. Kotelnikov[24], M.W. Krasny[28], H. Krehbiel[10], J. Kroseberg[36], D. Krücker[37], K. Krüger[10], A. Küpper[33], T. Kuhr[11], T. Kurča[34], W. Lachnit[10], R. Lahmann[10], D. Lamb[3], M.P.J. Landon[19], W. Lange[34], A. Lebedev[24], F. Lehner[10], V. Lemaitre[10], R. Lemrani[10], V. Lendermann[7], S. Levonian[10], M. Lindstroem[20], G. Lobo[26], E. Lobodzinska[10], V. Lubimov[23], S. Lüders[35], D. Lüke[7,10], L. Lytkin[12], N. Magnussen[33], H. Mahlke-Krüger[10], N. Malden[21], E. Malinovski[24], I. Malinovski[24], R. Maraček[25], P. Marage[4], J. Marks[13], R. Marshall[21], H.-U. Martyn[1], J. Martyniak[6], S.J. Maxfield[18], T.R. McMahon[18], A. Mehta[5], K. Meier[14], P. Merkel[10], F. Metlica[12], A. Meyer[10], H. Meyer[33], J. Meyer[10], P.-O. Meyer[2], S. Mikocki[6], D. Milstead[18], R. Mohr[25], S. Mohrdieck[11], M.N. Mondragon[7], F. Moreau[27], A. Morozov[8], J.V. Morris[5], D. Müller[36], K. Müller[13], P. Murín[16,42], V. Nagovizin[23], B. Naroska[11], J. Naumann[7], Th. Naumann[34], I. Négri[22], P.R. Newman[3], H.K. Nguyen[28], T.C. Nicholls[5], F. Niebergall[11], C. Niebuhr[10], O. Nix[14], G. Nowak[6], T. Nunnemann[12], J.E. Olsson[10], D. Ozerov[23], V. Panassik[8], C. Pascaud[26], S. Passaggio[35], G.D. Patel[18], E. Perez[9], J.P. Phillips[18], D. Pitzl[35], R. Pöschl[7], I. Potashnikova[12], B. Povh[12], K. Rabbertz[1], G. Rädel[9], J. Rauschenberger[11], P. Reimer[29], B. Reisert[25], D. Reyna[10], S. Riess[11], E. Rizvi[3], P. Robmann[36], R. Roosen[4], A. Rostovtsev[23,10], C. Royon[9], S. Rusakov[24], K. Rybicki[6], D.P.C. Sankey[5], J. Scheins[1], F.-P. Schilling[13], S. Schleif[14], P. Schleper[13], D. Schmidt[33], D. Schmidt[10], L. Schoeffel[9], T. Schörner[25], V. Schröder[10],

H.-C. Schultz-Coulon[10], F. Sefkow[36], V. Shekelyan[25], I. Sheviakov[24], L.N. Shtarkov[24], G. Siegmon[15], P. Sievers[13], Y. Sirois[27], T. Sloan[17], P. Smirnov[24], M. Smith[18], V. Solochenko[23], Y. Soloviev[24], V. Spaskov[8], A. Specka[27], H. Spitzer[11], R. Stamen[7], J. Steinhart[11], B. Stella[31], A. Stellberger[14], J. Stiewe[14], U. Straumann[13], W. Struczinski[2], J.P. Sutton[3], M. Swart[14], M. Taševský[29], V. Tchernyshov[23], S. Tchetchelnitski[23], G. Thompson[19], P.D. Thompson[3], N. Tobien[10], D. Traynor[19], P. Truöl[36], G. Tsipolitis[35], J. Turnau[6], J. Turney[19], E. Tzamariudaki[25], S. Udluft[25], A. Usik[24], S. Valkár[30], A. Valkárová[30], C. Vallée[22], A. Van Haecke[9], P. Van Mechelen[4], Y. Vazdik[24], G. Villet[9], S. von Dombrowski[36], K. Wacker[7], R. Wallny[13], T. Walter[36], B. Waugh[21], G. Weber[11], M. Weber[14], D. Wegener[7], A. Wegner[11], T. Wengler[13], M. Werner[13], L.R. West[3], G. White[17], S. Wiesand[33], T. Wilksen[10], M. Winde[34], G.-G. Winter[10], Ch. Wissing[7], M. Wobisch[2], H. Wollatz[10], E. Wünsch[10], J. Žáček[30], J. Zálešák[30], Z. Zhang[26], A. Zhokin[23], P. Zini[28], F. Zomer[26], J. Zsembery[9] and M. zur Nedden[10]

[1] *I. Physikalisches Institut der RWTH, Aachen, Germany*[a]
[2] *III. Physikalisches Institut der RWTH, Aachen, Germany*[a]
[3] *School of Physics and Space Research, University of Birmingham, Birmingham, UK*[b]
[4] *Inter-University Institute for High Energies ULB-VUB, Brussels; Universitaire Instelling Antwerpen, Wilrijk; Belgium*[c]
[5] *Rutherford Appleton Laboratory, Chilton, Didcot, UK*[b]
[6] *Institute for Nuclear Physics, Cracow, Poland*[d]
[7] *Institut für Physik, Universität Dortmund, Dortmund, Germany*[a]
[8] *Joint Institute for Nuclear Research, Dubna, Russia*
[9] *DSM/DAPNIA, CEA/Saclay, Gif-sur-Yvette, France*
[10] *DESY, Hamburg, Germany*[a]
[11] *II. Institut für Experimentalphysik, Universität Hamburg, Hamburg, Germany*[a]
[12] *Max-Planck-Institut für Kernphysik, Heidelberg, Germany*[a]
[13] *Physikalisches Institut, Universität Heidelberg, Heidelberg, Germany*[a]
[14] *Institut für Hochenergiephysik, Universität Heidelberg, Heidelberg, Germany*[a]
[15] *Institut für experimentelle und angewandte Physik, Universität Kiel, Kiel, Germany*[a]
[16] *Institute of Experimental Physics, Slovak Academy of Sciences, Košice, Slovak Republic*[f,j]
[17] *School of Physics and Chemistry, University of Lancaster, Lancaster, UK*[b]
[18] *Department of Physics, University of Liverpool, Liverpool, UK*[b]
[19] *Queen Mary and Westfield College, London, UK*[b]
[20] *Physics Department, University of Lund, Lund, Sweden*[g]
[21] *Department of Physics and Astronomy, University of Manchester, Manchester, UK*[b]
[22] *CPPM, Université d'Aix-Marseille II, IN2P3-CNRS, Marseille, France*
[23] *Institute for Theoretical and Experimental Physics, Moscow, Russia*
[24] *Lebedev Physical Institute, Moscow, Russia*[f,k]
[25] *Max-Planck-Institut für Physik, München, Germany*[a]
[26] *LAL, Université de Paris-Sud, IN2P3-CNRS, Orsay, France*
[27] *LPNHE, École Polytechnique, IN2P3-CNRS, Palaiseau, France*
[28] *LPNHE, Universités Paris VI and VII, IN2P3-CNRS, Paris, France*
[29] *Institute of Physics, Academy of Sciences of the Czech Republic, Praha, Czech Republic*[f,h]
[30] *Nuclear Center, Charles University, Praha, Czech Republic*[f,h]
[31] *INFN Roma 1 and Dipartimento di Fisica, Università Roma 3, Roma, Italy*

[32] *Paul Scherrer Institut, Villigen, Switzerland*
[33] *Fachbereich Physik, Bergische Universität Gesamthochschule Wuppertal, Wuppertal, Germany*[a]
[34] *DESY, Zeuthen, Germany*[a]
[35] *Institut für Teilchenphysik, ETH, Zürich, Switzerland*[i]
[36] *Physik-Institut der Universität Zürich, Zürich, Switzerland*[i]

[37] *Present address: Institut für Physik, Humboldt-Universität, Berlin, Germany*[a]
[38] *Also at Rechenzentrum, Bergische Universität Gesamthochschule Wuppertal, Wuppertal, Germany*[a]
[39] *Visitor from Yerevan Physics Institute, Armenia*
[40] *Also at Institut für Experimentelle Kernphysik, Universität Karlsruhe, Karlsruhe, Germany*
[41] *On leave from CINVESTAV, México*
[42] *Also at University of P.J. Šafárik, SK-04154 Košice, Slovak Republic*
[43] *Dept. Fis. Ap. CINVESTAV, Mérida, Yucatán, México*
† *Deceased*

[a] *Supported by the Bundesministerium für Bildung, Wissenschaft, Forschung und Technologie, FRG, under contract numbers 7AC17P, 7AC47P, 7DO55P, 7HH17I, 7HH27P, 7HD17P, 7HD27P, 7KI17I, 6MP17I and 7WT87P*
[b] *Supported by the UK Particle Physics and Astronomy Research Council, and formerly by the UK Science and Engineering Research Council*
[c] *Supported by FNRS-FWO, IISN-IIKW*
[d] *Partially supported by the Polish State Committee for Scientific Research, grant no. 115/E-343/SPUB/P03/002/97 and grant no. 2P03B 055 13*
[e] *Supported in part by US DOE grant DE F603 91ER40674*
[f] *Supported by the Deutsche Forschungsgemeinschaft*
[g] *Supported by the Swedish Natural Science Research Council*
[h] *Supported by GA ČR grant no. 202/96/0214, GA AV ČR grant no. A1010821 and GA UK grant no. 177*
[i] *Supported by the Swiss National Science Foundation*
[j] *Supported by VEGA SR grant no. 2/5167/98*
[k] *Supported by Russian Foundation for Basic Research grant no. 96-02-00019*
[l] *Supported by the Alexander von Humboldt Foundation*

1 Introduction

Hadronic final state analyses in Deep-Inelastic Scattering (DIS) interactions at HERA allow novel stringent tests of the physics of Quantum Chromodynamics (QCD), the theory of the strong interactions, in a kinematical region of high parton densities which so far has not been accessible [1, 2, 3, 4]. The high Center of Mass System (CMS) energy ($\sim$ 300 GeV) of the HERA collider allows a region in Bjorken-x of $\sim 10^{-5} - 10^{-4}$ to be reached while keeping the momentum transfer, Q^2, larger than a few GeV^2, hence remaining in the regime of perturbative QCD (pQCD). In DIS a parton in the proton can induce a QCD cascade consisting of several subsequent parton emissions before the final parton interacts with the virtual photon. The multiplicity and the x distribution of these emitted partons differ significantly in different approximations of QCD dynamics at small x.

At low x, pQCD evolution is complicated by the occurrence of two large logarithms in the evolution equations, namely $\ln 1/x$ and $\ln Q^2$. In contrast, in the better tested region of pQCD at larger x a summation of the leading $\ln Q^2$ terms is sufficient. A complete perturbative treatment in the low-x region is not yet available, and different approximations are made resulting in different parton dynamics. At high Q^2 and high x pQCD requires the resummation of contributions of $\alpha_s \ln(Q^2/Q_0^2)$ terms, yielding the DGLAP (Dokshitzer-Gribov-Lipatov-Altarelli-Parisi) [5] evolution equations. However at small x the contribution of large leading $\ln 1/x$ terms may become important. Resummation of these terms leads to the BFKL (Balitsky-Fadin-Kuraev-Lipatov) [6] evolution equation. Hence a pertinent and exciting question is whether these $\ln 1/x$ contributions to the parton evolution can be observed experimentally.

Differences between different dynamical assumptions for the parton cascade are expected to be most prominent in the phase space region towards the proton remnant direction, i.e. away from the scattered quark. Here we investigate the region of central rapidity in the CMS system of the virtual photon and the proton. In the HERA laboratory frame this corresponds to a region of small polar angles and has been generically termed "forward region"[1]. In previous H1 analyses results have been presented on forward jet and forward inclusive charged and neutral pion production [7, 8], based on data collected in 1994. A measurement on forward jet production has been presented by the ZEUS collaboration [9]. In this paper we study forward single π° production for a considerably larger data sample than that of [8], collected in 1996 and which allows the selection of particles with larger transverse momentum, p_T. The production of high p_T particles is strongly correlated with the emission of hard partons in QCD and is therefore sensitive to the dynamics of the strong interaction [10, 11, 12]. An advantage of studying single particles, as opposed to jets, is that no jet algorithm is needed and the potential to reach smaller angles than is possible with jets with broad spatial extent. Furthermore, theoretical calculations at the parton level can be convoluted with known fragmentation functions[13], allowing a direct comparison of the measurements and theory. The selection of high p_T particles is also inspired by the proposal of Mueller [1] to select events where the photon virtuality Q^2 and transverse momentum squared of the parton emitted in the parton cascade, k_T^2, are of similar magnitude, thereby suppressing the k_T ordered DGLAP evolution with respect to the non-k_T ordered BFKL evolution.

[1] H1 uses a right-handed coordinate system with the z-axis defined by the incident proton beam and the y-axis pointing upward.

In this analysis π°'s are selected in DIS events at low x in the region of momentum transfer $2 < Q^2 < 70$ GeV^2. The π°'s are required to have a polar angle in the lab frame between 5° and 25°, and transverse momentum larger than 2.5 GeV in the hadronic CMS (contrary to the analysis in [8], where a minimum transverse momentum of 1 GeV was required in the laboratory frame). Large transverse momenta in the hadronic CMS, as opposed to the laboratory system, are more directly related to hard subprocesses, since in the quark parton model picture the current quark has zero p_T in the hadronic CMS. The increased transverse momentum cut enhances the sensitivity to hard parton emission in the QCD cascade and provides a hard scale for perturbative calculations. It also reduces significantly the influence of soft hadronization.

A calculation based on pQCD which uses the BFKL formalism for the perturbative part, and fragmentation functions for the hadronization, is available [4] and will be compared with the data. In addition, models using $\mathcal{O}(\alpha_s)$ QCD matrix elements and parton cascades according to DGLAP evolution, and colour string hadronization, will be compared with the data.

2 Experimental Apparatus

A detailed description of the H1 detector can be found elsewhere [14]. The following section briefly describes the components of the detector relevant for this analysis.

The hadronic energy flow and the scattered electron are measured with a liquid argon (LAr) calorimeter and a backward SPACAL calorimeter, respectively. The LAr calorimeter [15] extends over the polar angle range $4^\circ < \theta < 154^\circ$ with full azimuthal coverage. It consists of an electromagnetic section with lead absorbers and a hadronic section with steel absorbers. With about $44\,000$ cells in total, both sections are highly segmented in the transverse and the longitudinal direction, in particular in the forward region of the detector. The total depth of both sections varies between 4.5 and 8 interaction lengths in the region $4^\circ < \theta < 128^\circ$. Test beam measurements of the LAr calorimeter modules showed an energy resolution of $\sigma_E/E \approx 0.50/\sqrt{E\,[\mathrm{GeV}]} \oplus 0.02$ for charged pions and of $\sigma_E/E \approx 0.12/\sqrt{E\,[\mathrm{GeV}]} \oplus 0.01$ for electrons [15]. The hadronic energy measurement is performed by applying a weighting technique in order to account for the non-compensating nature of the calorimeter. The absolute scale of the hadronic energy is presently known to 4%. The scale uncertainty for electromagnetic energies is 3% [16] for the forward region relevant for this analysis.

The SPACAL [17] is a lead/scintillating fibre calorimeter which covers the region $153^\circ < \theta < 177.8^\circ$ with an electromagnetic section and a hadronic section. The energy resolution for electrons is $7.5\,\%/\sqrt{E} \oplus 2.5\,\%$, the energy resolution for hadrons is $\sim 30\%$. The energy scale uncertainties are 1% and 7% for the electrons and hadrons respectively. The timing resolution of better than 1 ns in both sections of the SPACAL is exploited to form a trigger decision and reject background.

The calorimeters are surrounded by a superconducting solenoid providing a uniform magnetic field of 1.15 T parallel to the beam axis in the tracking region. Charged particle tracks are measured in the central tracker (CT) covering the polar angular range $25^\circ < \theta < 155^\circ$ and the forward tracking (FT) system, covering the polar angular range $5^\circ < \theta < 25^\circ$. The CT consists of inner and outer cylindrical jet chambers, z-drift chambers and proportional chambers. The

jet chambers, mounted concentrically around the beam line, provide up to 65 space points in the radial plane for tracks with sufficiently large transverse momentum.

A backward drift chamber (BDC) in front of the SPACAL with an angular acceptance of $151^\circ < \theta < 177.5^\circ$ serves to identify electron candidates and to precisely measure their direction. Using information from the BDC, the SPACAL and the reconstructed event vertex the polar angle of the scattered electron is known to about 0.7 mrad.

The luminosity is measured using the reaction $ep \to ep\gamma$ with two TlCl/TlBr crystal calorimeters installed in the HERA tunnel. The electron tagger is located at $z = -33$ m and the photon tagger at $z = -103$ m from the interaction point in the direction of the outgoing electron beam.

3 Theoretical Predictions

Predictions for final state observables are available from Monte Carlo models using $\mathcal{O}(\alpha_s)$ matrix elements and parton cascades according to the DGLAP evolution, and from numerical calculations based upon the BFKL formalism. In the following we describe the models and calculations used.

3.1 Phenomenological QCD Models

Implementations of $\mathcal{O}(\alpha_s)$ matrix elements complemented by parton showers based on the DGLAP splitting functions are available in the programs LEPTO6.5 [18] and HERWIG5.9 [19]. The factorization and renormalization scales are set to Q^2. The predictions of these models should be valid in the region: $\alpha_s(Q^2)\ln(Q^2/Q_0^2) \sim 1$ and $\alpha_s(Q^2)\ln(1/x) \ll 1$. In LEPTO the Lund string model as implemented in JETSET7.4 [20] is used to describe hadronization processes. LEPTO includes soft colour interactions in the final state which can lead to events with a large rapidity gap. HERWIG differs from LEPTO in that it also considers interference effects due to colour coherence and uses the cluster fragmentation model for hadronization. The versions of LEPTO6.5 and HERWIG5.9 used consider only DIS processes in which the virtual photon is point-like.

Recently a model has been proposed (RAPGAP2.06 [21]) which is also based on the DGLAP formalism but includes contributions from processes in which the virtual photon entering the scattering process can be resolved. The relative contribution from resolved photon processes depends on the scale at which the virtual photon is probed. As in [22] the factorization and renormalization scale in this paper is taken to be $Q^2 + p_T^2$ (p_T^2 of the partons from the hard subprocess).

The model calculations in this paper were made with the CTEQ4M [23] parton densities for the proton and the SAS-1D [24] parton densities for the virtual photon. QED corrections are determined with the Monte Carlo program DJANGO6.2 [25]. The contribution of photons emitted in the forward direction from QED processes originating from the quarks in the proton, were found to be negligible.

In a previous paper [8] we compared the results with ARIADNE [26] and LDCMC [27]. ARIADNE provides an implementation of the Colour Dipole Model (CDM) of a chain of independently radiating dipoles formed by emitted gluons [28]. Unlike LEPTO, the cascade of the CDM is not ordered in transverse momentum. For the present analysis it was confirmed that the predictions depend strongly on the parameters controlling the "size" of the diquark and photon, and are therefore not explicitly compared with data in this paper[2]. The linked dipole chain (LDC) model [29] is a reformulation of the CCFM [30] equation, which forms a bridge between the BFKL and DGLAP approaches. Calculations of the hadronic final state based on this approach are available with the LDCMC 1.0 Monte Carlo which matches exact first order matrix elements with the LDC-prescribed initial and final state parton emissions. The model however failed to describe the data in [8] and is therefore not considered further in this paper.

3.2 BFKL Calculation

Recently π° cross-sections have been calculated [4] based on a modified BFKL evolution equation in order $\mathcal{O}(\alpha_s)$ convoluted with π° fragmentation functions. The modified evolution equations include the so called "consistency constraint" [31, 32] which limits the gluon emission at each vertex in the cascade to the kinematically allowed region. It is argued that this constraint embodies a major part of the non-leading $\ln(1/x)$ contributions to the BFKL equation, which have been found to be very important [33]. The predictions of this modified BFKL equation are therefore expected to be more reliable than those without this constraint. The parton densities and fragmentation functions used in the calculation are taken from [34] and [13] respectively. In this paper we compare "set (iii)" of [4] to the data. In this set the scale for the strong coupling constant α_S is taken to be the transverse momentum squared of the emitted partons, k_T^2, and the infrared cut-off in the modified BFKL equation is taken to be 0.5 GeV^2. Calculations with these parameters give a fair description of the forward jet cross-sections from [8] when taking into account hadronization corrections. The predictions are labelled "mod LO BFKL" in the figures.

4 Measurement

4.1 Data Selection

The analysis is based on data representing an integrated luminosity of $\mathcal{L} = 5.8\ \mathrm{pb}^{-1}$ taken by H1 during 1996. Deep-inelastic scattering events are selected and the event kinematics are calculated from the polar angle and the energy of the scattered positron. The four momentum transfer squared, Q^2, and the inelasticity, y, are related to these quantities (neglecting the positron mass) by $Q^2 = 4\,E_e\,E_l\cos^2\frac{\theta_e}{2}$ and $y = 1 - \frac{E_e}{E_l}\sin^2\frac{\theta_e}{2}$, where E_l and E_e are the energies of the incoming and the scattered positron respectively, and θ_e is the polar angle of the scattered positron. Bjorken-x is then given by $x = Q^2 / (\,y \cdot s\,)$, where s is the square of the ep center of mass energy.

[2] A good description of the data presented in this paper can be achieved (using ARIADNE4.10) e.g. choosing PARA(10)=1.7 and PARA(14)=1.0 [12].

Experimentally the scattered positron is defined to be the highest energy cluster, i.e. localized energy deposit, in the SPACAL with a cluster radius of less than 3.5 cm and an associated track in the BDC. Experimental requirements based on the energy and the polar angle of the scattered positron are used during the preselection but these are superseded by stronger kinematic cuts which restrict the data to the range $0.1 < y < 0.6$ and $2 < Q^2 < 70$ GeV^2. The restricted y-range ensures that the particles from the current quark are detected in the central detector, and not in the forward region, and that the DIS kinematics can be well determined from the measurement of the scattered positron. Photoproduction background is further reduced to a negligible level by requiring $35 < \sum_j (E_j - p_{z,j}) < 70$ GeV [35] with E_j and $p_{z,j}$ the energy and longitudinal momentum of a particle respectively, and where the sum extends over all detected particles in the event, except for those in the small angle electron and photon tagger. The reconstructed primary event vertex must have a z coordinate not more than 35 cm away from the nominal interaction point. The trigger is based on energy depositions in the SPACAL and demands multiple track activity in the central tracker. For the events used in this analysis the efficiency of this trigger is around 80%, determined using data from an independent second trigger.

After the selection about 600K events are available for further analysis.

4.2 Forward π°-Meson Selection

A measurement of particle production at mid-rapidity in the hadronic CMS system requires small forward angles in the lab system. It is difficult to identify individual charged particles in the forward direction in an environment with a high density of charged particles. However the finely segmented H1 LAr calorimeter allows the measurement of π°'s down to very small angles. They are measured using the dominant decay channel $\pi^\circ \to 2\gamma$. The π° candidates are selected in the region $5^\circ < \theta_\pi < 25^\circ$, where θ_π is the polar angle of the produced π°. Candidates are required to have an energy such that $x_\pi = E_\pi / E_{proton} > 0.01$, with E_{proton} the proton beam energy (820 GeV), and a transverse momentum in the hadronic CMS, $p^*_{T,\pi}$, greater than 2.5 GeV. At the high π° energies considered here, the two photons from the decay cannot be separated, but appear as one object (cluster) in the calorimetric response. Therefore, the standard method to identify π°-mesons by reconstructing the invariant mass from the separate measurement of the two decay photons is not applicable.

In this paper, a detailed analysis of the longitudinal and transverse shape of the energy depositions is performed to separate electromagnetic from hadronic showers. This approach is based on the compact nature of electromagnetic showers as opposed to showers of hadronic origin, which are broader. The analysis of shower profiles is made possible by the fine granularity of the calorimeter in the forward direction. It has a typical lateral cell size of 3.5×3.5 cm^2. This can be compared to the mean Moliere radius $\bar{R}_m$ which is 3.6 cm and the mean radiation length $\bar{X}_0$ which is 1.6 cm. The calorimeter has a four-fold longitudinal segmentation for the electromagnetic section which has a thickness of 20 to 25 radiation lengths X_0. The main experimental challenge in this analysis is the high activity in this region of phase space, with hadronic showers "masking" the clear electromagnetic signature from the $\pi^\circ \to 2\gamma$ decay. The overlap of a π° induced cluster with another hadron is mainly responsible for losses of π° detection efficiency,

since the distortion of the shower shape estimators it causes will, in many cases, lead to the rejection of the cluster candidate.

The reconstruction of LAr data is optimized to contain all the energy of an electromagnetic shower in one cluster [14]. A π°-meson candidate is required to be a cluster with more than 90 $\%$ of its energy deposited in the electromagnetic part of the LAr calorimeter. A "hot" core consisting of the most energetic group of contiguous electromagnetic calorimeter cells of a cluster, which must include the hottest cell, is defined for each candidate [36]. More than 50 $\%$ of the cluster energy is required to be deposited in this core. The lateral spread of the shower is quantified in terms of lateral shower moments calculated relative to the shower's principal axis [36] and required to be less than 4 cm [12]. The longitudinal shower shape is used as a selection criterion via the fraction of the shower's energy deposited in each layer of cells in the electromagnetic part of the calorimeter. The precise specifications of these layers can be found in [36]. The part of the cluster's energy measured in the second layer minus that measured in the fourth layer is required to be more than 40% of the total cluster energy. This selects showers which start to develop close to the calorimeter surface and are well contained in the electromagnetic part of the calorimeter, as expected for showers of electromagnetic origin. As mentioned above, with this selection one cannot distinguish photons from a π°-meson decay and photons from other sources. The high energy required in the selection, however, ensures that contributions from sources other than high energy π°-mesons (such as prompt photon production) are at a negligible level [37]. The influence of η-meson production is corrected for in the analysis. Uncertainties in the relative η and π° production rates in the Monte Carlo models used have been studied and were found to have an negligible effect on the results.

With this selection about 1700 (600) π° candidates are found in the kinematic range $5^\circ < \theta_\pi < 25^\circ$, $x_\pi > 0.01$ and $p^\star_{T,\pi} > 2.5$ (3.5) GeV, with a detection efficiency better than 45%. Monte Carlo studies, using a detailed simulation of the H1 detector for a sample of DIS events, yield a purity of about 70% for the selected π°-meson sample. The impurities are due to misidentified hadrons and from secondary interactions of charged hadrons with passive material in the detector (between one and two radiation lengths in the forward region). These studies show that less than 10$\%$ of the selected π° candidates stem from secondary scattering of charged hadrons with passive material in the forward region, where the amount of material between the interaction point and the calorimeter surface is largest.

The determination of the π° acceptance and purity depends only on the particle density and energies in the forward calorimeter. To ensure that the different Monte Carlo models used are in reasonable agreement with the data in this respect the transverse energy flow, E_T, around the π° candidate clusters was studied in detail. Both the E_T flow and the E_T spectra in the tail of the E_T flow distributions are reasonably well described by the models used to determine the detector corrections [12]. Of the two models used, however, ARIADNE showed a higher particle density while LEPTO has a lower particle density than the data. Remaining differences of the detector corrections determined with the two Monte Carlo models are therefore used to estimate the systematic error. When the energy and transverse momentum requirements are lowered, the two photons from the π° decay become separable and a clear π° mass peak can be observed which is also well reproduced by the H1 detector simulation. The same method of selecting π°-mesons as outlined above was used in a previous H1 analysis [8], where a measurement of charged particles in the same region was also performed. The measured π° cross-sections were found to agree well with the average of the π^+ and π^- cross sections. Furthermore, the results

of the analysis of the 1994 data are found to be in good agreement with the present analysis in their overlapping phase space regions.

5 Results

The experimental results of the analysis are presented as differential ep cross-sections of forward π°-meson production as a function of Q^2, and as a function of x, η_π and $p^\star_{T,\pi}$ in three regions of Q^2 for $p^\star_{T,\pi} > 2.5$ GeV. The pseudorapidity η_π is given by $-\ln[\tan(\theta/2)]$ with θ being the polar angle of the π° in the laboratory frame. In addition the π° cross-sections as a function of x and Q^2 are measured for data with the threshold of the π° transverse momentum increased to $p^\star_{T,\pi} > 3.5$ GeV. An increased $p^\star_{T,\pi}$ threshold is expected to enhance the sensitivity to hard parton emission in the parton cascade. The phase space is given by $0.1 < y < 0.6$, $2 < Q^2 < 70$ GeV^2, $5^\circ < \theta_\pi < 25^\circ$ and $x_\pi = E_\pi/E_{proton} > 0.01$, in addition to the $p^\star_{T,\pi}$ thresholds given above. θ_π, E_π and E_{proton} are measured in the H1 laboratory frame; $p^\star_{T,\pi}$ is calculated in the hadronic CMS. The measurement extends down to $x = 4{\cdot}10^{-5}$, covering two orders of magnitude in Bjorken-x.

All observables are corrected for detector effects and for the influence of QED radiation by a bin-by-bin unfolding procedure. The detector effects include the efficiency, purity and acceptance of the π°-meson identification as well as contributions from secondary scattering in passive material. The correction functions are obtained with two different models (ARIADNE and LEPTO) and detailed detector simulation. The final correction is performed with the average of the two models. The remaining background from photoproduction in the data sample has been studied using a sample of photoproduction Monte Carlo events (PHOJET [38]) representing an integrated luminosity of about 1 pb^{-1}. The contribution from such events is found to be negligible in all bins.

The typical total systematic uncertainty is 15-25$\%$, compared to a statistical uncertainty of about 10$\%$. Contributions to the systematic error include: the uncertainty of the luminosity measurement (1.8$\%$), the statistical uncertainty in the determination of the trigger efficiency (5$\%$), the uncertainty of the electromagnetic energy scale of the LAr (3%) and the SPACAL (1%) calorimeters which each contribute 5-10$\%$, the variation of π°-meson selection and acceptance requirements within the resolution of the reconstructed quantities (5-10$\%$), and the model dependence of the bin-by-bin correction procedure using differences between ARIADNE and LEPTO (5-10$\%$).

The cross-sections as a function of x, shown in Fig. 1(a), exhibit a strong rise towards small x. In this and the following figures the inner error bars give the statistical errors, while the outer error bars give the statistical and systematical error added quadratically. It is of interest to note that the rise in x in Fig. 1(a) is similar to the rise of the total inclusive cross-section as measured e.g. in [39]. This is demonstrated in Fig. 1(b), which shows the rate of π°-meson production in DIS as a function of x obtained by dividing the cross-section shown in Fig. 1(a) by the inclusive ep cross-section in each bin of x and Q^2 . The inclusive cross-section is calculated by integrating the H1 QCD fit to the 1996 structure function data as presented in [39] for every bin of inclusive π°-meson cross-sections. Note, however, that the π° rate increases with increasing Q^2. The x-independence seen in Fig. 1(b) in a fixed Q^2 interval implies that the π° rate for

particles with a p_T above the cut-off and within the selected kinematical region, is independent of W, the hadronic invariant mass of the photon-proton system.

The shapes of $d\sigma_\pi/d\eta_\pi$ and $d\sigma_\pi/dp^\star_{T,\pi}$ (Fig. 2) show no significant dependence on Q^2 . The measurements of the latter extend to values of transverse momenta as high as 8 GeV. Since η_π is measured in the laboratory frame, mid-rapidity in the hadronic CMS corresponds approximately to $\eta_\pi = 2$ in Figure 2 (a). Figure 3 shows the inclusive π°-meson cross-section as a function of Q^2 . The cross-section falls steeply with increasing Q^2. Figure 4 finally shows $d\sigma_\pi/dQ^2$ and $d\sigma_\pi/dx$ for the higher threshold of $p^\star_{T,\pi} > 3.5$ GeV. No significant change in shape of the distributions occurs when the $p^\star_{T,\pi}$ threshold is raised, but the cross-sections are reduced by about a factor of three.

All differential cross-sections are compared to three predictions based on different QCD approximations. The DGLAP prediction for pointlike virtual photon scattering (including parton showers) as given by LEPTO6.5 falls clearly below the data. There is still a fair agreement with data for the highest x and Q^2 bins, shown in Fig. 1(a) and Fig. 3, but differences occur in the low-x region. These are as large as a factor of five in the lowest x region. LEPTO also fails to describe the ratio in Fig. 1(b), and shows a strong decrease with decreasing x. The mechanism of emitting partons according to the DGLAP splitting functions, combined with pointlike virtual photon scattering only, is clearly not supported by the data, in particular at low x. The LEPTO prediction is based on about seven times the integrated luminosity of the data. Comparisons to HERWIG5.9 (not shown) lead to similar conclusions [12].

A considerable improvement of the description of the data is achieved by a model which considers additional processes where the virtual photon entering the scattering process is resolved. This approach can be regarded as an effective resummation of higher order corrections. It also provides a smooth transition towards the limit of $Q^2 = 0$, i.e. photoproduction, where resolved processes dominate in the HERA regime. Such a prediction is provided by RAPGAP2.06 [21]. In Fig. 1(a) RAPGAP2.06 predicts a cross-sections very close to the measured distributions with the exception of the lowest Q^2 bin where the prediction is too low. All predicted cross-sections increase by up to 30% when the scale in the hard scattering is increased from $Q^2 + p_T^2$ to $Q^2 + 4p_T^2$ [12], and therefore do not improve the overall description significantly. Hence RAPGAP, with the parton distributions used here, does not describe the low-x behaviour of the data over the full range. The RAPGAP prediction is based on approximately four times the integrated luminosity of the data.

The ARIADNE model (not shown), with parameters as given before, can describe the data presented in this paper [12], but it remains to be shown whether this choice allows for a consistent description of other aspects of the DIS final state data. Moreover, a moderate variation of these parameters leads to large changes in the prediction.

Next we compare the data with a prediction of the π°-meson cross-section based on a modified LO BFKL parton calculation convoluted with π° fragmentation functions. The predictions obtained with these calculations turn out to be in good agreement with the neutral pion cross-sections measured in most of the available phase space, but are below the data at the lowest values of Q^2. The calculation also describes well the ratio shown in Fig. 1(b), except possibly at the largest Q^2, x bin. This ratio has been calculated by using the corresponding prediction for the inclusive cross section, based on the BFKL formalism [32].

The BFKL predictions involve a cut-off parameter in the transverse momentum squared k_T^2 of the partons: k_0^2=0.5 GeV^2 and a choice of renormalization scale. It is shown in [4] that a variation of k_0^2 by a factor of two leads to less than a 10% change of the cross-sections. The scale dependence is larger; a change from k_T^2 to $k_T^2/4$ leads to an approximate increase of 60% of the cross-sections. This affects mostly the normalization, but not the shape of the distributions.

The good agreement between this prediction and the data suggests that the modified BFKL evolution equation, using the consistency constraints, is a good approximation for low-x evolution in the considered phase space. This, in turn, can then be interpreted as a sign of the experimental manifestation of leading $\ln 1/x$ terms which are anticipated in pQCD evolution.

6 Conclusions

Differential cross-sections of forward π° production have been measured for particles with $p^\star_{T,\pi} > 2.5$ (3.5) GeV, $5^\circ < \theta_\pi < 25^\circ$ and $x_\pi = E_\pi/E_{proton} > 0.01$, for DIS events with $0.1 < y < 0.6$ and $2 < Q^2 < 70$ GeV^2. The data are sensitive to QCD parton dynamics at low x (high parton density) and mid-rapidity in the hadronic CMS system. They discriminate between different approximations to QCD evolution in the new regime opened up by HERA. The data show a strong rise of the cross section with decreasing x. This rise is similar to the rise of the inclusive cross section.

Models using $\mathcal{O}(\alpha_s)$ QCD matrix elements and parton cascades according to the DGLAP splitting functions cannot describe the differential neutral pion cross-sections at low x. Inclusion of processes in which the virtual photon is resolved improves the agreement with the data, but does not provide a satisfactory description in the full x and Q^2 range. A calculation based on the BFKL formalism is in good agreement with the data, particularly for the shape description, but the absolute normalization remains strongly affected by the scale uncertainty. So far the data in the phase space selected in this analysis could not be confronted with a next-to-leading (NLO) order prediction – either for DGLAP or for BFKL. More definite conclusions therefore have to be delayed until such calculations become available.

Acknowledgments

We wish to thank A.D. Martin, J.J. Outhwaite and A.M. Stasto for useful discussions. We are grateful to the HERA machine group whose outstanding efforts have made and continue to make this experiment possible. We thank the engineers and technicians for their work constructing and maintaining the H1 detector, our funding agencies for financial support, the DESY technical staff for continual assistance and the DESY directorate for the hospitality which they extend to the non-DESY members of the collaboration.

References

[1] A.H. Mueller, Nucl. Phys. B (Proc. Suppl.) **18C** (1990) 125;
J. Phys. **G17** (1991) 1443.

[2] J. Kwieciński, A.D. Martin, P.J. Sutton, Phys. Rev. **D46** (1992) 921.

[3] J. Bartels, A. De Roeck, M. Loewe, Z. Phys. **C54** (1992) 635;
W.K. Tang, Phys. Lett. **B278** (1992) 363.

[4] J. Kwiecinski, A.D. Martin, J.J. Outhwaite, hep-ph/9903439, DTP-99-28, to be published in Eur. Phys. J. **C**; A.M. Stasto, private communication.

[5] V.N. Gribov, L.N. Lipatov, Sov. J. Nucl. Phys. **15** (1972) 438 and 675;
Yu. L. Dokshitzer, Sov. Phys. JETP **46** (1977) 641;
G. Altarelli, G. Parisi, Nucl. Phys. **126** (1977) 297.

[6] E.A. Kuraev, L.N. Lipatov, V.S. Fadin, Sov. Phys. JETP **45** (1972) 199; Y.Y. Balitsky, L.N. Lipatov, Sov. J. Nucl. Phys. **28** (1978) 822.

[7] H1 Collab., S. Aid et al., Phys. Lett. **B356** (1995) 118.

[8] H1 Collab., C. Adloff et al., Nucl. Phys. **B538** (1999) 3.

[9] ZEUS Collab., J. Breitweg et al., Eur. Phys. J. **C6** (1999) 239.

[10] M. Kuhlen, Phys. Lett. **B382** (1996) 441.

[11] H1 Collab., C. Adloff et al., Nucl. Phys. **B485** (1997) 3.

[12] T. Wengler, PhD thesis, University of Heidelberg, January 1999, DESY-THESIS-1999-011.

[13] J. Binnewies, B.A. Kniehl, G. Kramer, Phys.Rev. **D52** (1995) 4947.

[14] H1 Collab., I. Abt et al., Nucl. Instr. and Meth. **A386** (1997) 310 and
Nucl. Instr. and Meth. **A386** (1997) 348.

[15] H1 Calorimeter Group, B. Andrieu et al., Nucl. Instr. and Meth. **A336** (1993) 460 and 499.

[16] H1. Collab., Measurement of the Neutral and Charged Current Cross-Sections in Positron-Proton Collisions at Large Momentum Transfer, in preparation.

[17] H1 SPACAL Group, R.D. Appuhn, et al., Nucl. Instr. and Meth. **A386** (1997) 397.

[18] G. Ingelman, A. Edin, J. Rathsman, Comp. Phys. Comm. **101** (1997) 108.

[19] G. Marchesini et al., Comp. Phys. Comm. **67** (1992) 465;
M.H. Seymour, Nucl. Phys. **B436** (1995) 443.

[20] T. Sjöstrand, Comp. Phys. Comm. **39** (1986) 347;
T. Sjöstrand, M. Bengtsson, ibid. **43** (1987) 367.

[21] H. Jung, Comp. Phys. Comm. **86** (1995) 147.

[22] H. Jung, L. Jönsson, H. Kuester, DESY 98-051, hep-ph/9805396.

[23] CTEQ Collab., H.L. Lai et al., Phys.Rev. **D55** (1997) 1280.

[24] G.A. Schuler, T. Sjostrand, Phys. Lett. **B376** (1996) 193.

[25] K. Charchula, G. Schuler, H. Spiesberger, Comp. Phys. Comm. **81** (1994) 381.

[26] L. Lönnblad, Comp. Phys. Comm. **71** (1992) 15.

[27] H. Kharraziha, L. Lönnblad, JHEP **9803** (1998) 6.

[28] G. Gustafson, U. Pettersson, Nucl. Phys. **B306** (1988) 746;
G. Gustafson, Phys. Lett. **B175** (1986) 453;
B. Andersson, G. Gustafson, L. Lönnblad, U. Pettersson, Z. Phys. **C43** (1989) 625.

[29] B. Andersson, G. Gustafson, J. Samuelsson, Nucl. Phys. **B467** (1996) 443;
B. Andersson, G. Gustafson, H. Kharraziha, J. Samuelsson, Z. Phys. **C71** (1996) 613.

[30] M. Ciafaloni, Nucl. Phys. **B296** (1988) 49;
S. Catani, F. Fiorani, G. Marchesini, Phys. Lett. **234B** (1990) 339 and
Nucl. Phys. **B336** (1990) 18.

[31] J. Kwiecinski, A.D. Martin, P.J. Sutton, Z. Phys. **C71** (1996) 585.

[32] J. Kwiecinski, A.D. Martin, A.M. Stasto, Phys. Rev. **D56** (1997) 3991.

[33] V.S. Fadin, L.N. Lipatov, Phys. Lett. **B429** (1998) 127.

[34] A.D. Martin, R.G. Roberts, W.J. Stirling, R.S. Thorne, Eur. Phys. J. **C4** (1998) 463.

[35] H1 Collab., S. Aid et al., Nucl. Phys. **B470** (1996) 3.

[36] H1 Calorimeter Group, B. Andrieu, et al., Nucl. Instr. and Meth. **A334** (1994) 492.

[37] J. Kwiecinski, S.C. Lang, A.D. Martin, Phys. Rev. **D55** (1997) 1273.

[38] R. Engel, Z. Phys. **C66** (1995) 203;
R. Engel, J. Ranft, Phys. Rev. **D54** (1996) 4244.

[39] H1 Collab., C. Adloff et al., Contributed paper (260) to HEP97 Jerusalem, August 9-26, 1997.

$x \cdot 10^4$	$(\frac{d\sigma_\pi}{dx})^{\pm stat}_{\pm tot}$ /nb	η_π	$(\frac{d\sigma_\pi}{d\eta_\pi})^{\pm stat}_{\pm tot}$ /pb	$p^\star_{T,\pi}$ /GeV	$(\frac{d\sigma_\pi}{dp^\star_{T,\pi}})^{\pm stat}_{\pm tot}$ /$\frac{\text{pb}}{\text{GeV}}$
$2.0 < Q^2 < 4.5$ GeV^2		$p^\star_{T,\pi} > 2.5$ GeV (hcms)			
0.42 – 0.79	$1189^{\pm 134}_{\pm 188}$	1.50 – 1.93	$141^{\pm 16}_{\pm 28}$	2.50 – 2.80	$187^{\pm 20}_{\pm 92}$
0.79 – 1.1	$1261^{\pm 143}_{\pm 253}$	1.93 – 2.23	$165^{\pm 20}_{\pm 31}$	2.80 – 3.30	$132^{\pm 13}_{\pm 22}$
1.1 – 1.7	$970^{\pm 96}_{\pm 201}$	2.23 – 2.56	$129^{\pm 15}_{\pm 29}$	3.30 – 4.00	$65.3^{\pm 7.5}_{\pm 17.5}$
1.7 – 2.5	$609^{\pm 75}_{\pm 121}$	2.56 – 2.85	$108^{\pm 13}_{\pm 26}$	4.00 – 5.20	$25.1^{\pm 3.4}_{\pm 4.2}$
2.5 – 4.2	$160^{\pm 27}_{\pm 52}$	2.85 – 3.13	$111^{\pm 15}_{\pm 26}$	5.20 – 8.00	$6.48^{\pm 1.23}_{\pm 1.86}$
$4.5 < Q^2 < 15.0$ GeV^2		$p^\star_{T,\pi} > 2.5$ GeV (hcms)			
1.1 – 2.0	$398^{\pm 43}_{\pm 61}$	1.50 – 1.91	$103^{\pm 11}_{\pm 16}$	2.50 – 2.80	$157^{\pm 15}_{\pm 74}$
2.0 – 2.9	$366^{\pm 41}_{\pm 59}$	1.91 – 2.22	$145^{\pm 15}_{\pm 29}$	2.80 – 3.40	$93.5^{\pm 7.8}_{\pm 21.7}$
2.9 – 3.9	$337^{\pm 39}_{\pm 64}$	2.22 – 2.50	$131^{\pm 14}_{\pm 21}$	3.40 – 4.10	$56.9^{\pm 6.4}_{\pm 9.5}$
3.9 – 5.5	$193^{\pm 21}_{\pm 34}$	2.50 – 2.82	$115^{\pm 12}_{\pm 21}$	4.10 – 5.20	$16.6^{\pm 2.4}_{\pm 3.8}$
5.5 – 11	$63.5^{\pm 6.8}_{\pm 13.8}$	2.82 – 3.13	$89.0^{\pm 10.2}_{\pm 22.1}$	5.20 – 8.00	$4.45^{\pm 0.75}_{\pm 1.18}$
$15.0 < Q^2 < 70.0$ GeV^2		$p^\star_{T,\pi} > 2.5$ GeV (hcms)			
3.9 – 7.9	$72.4^{\pm 8.7}_{\pm 16.8}$	1.50 – 1.93	$66.2^{\pm 7.9}_{\pm 14.9}$	2.50 – 2.90	$89.0^{\pm 9.5}_{\pm 34.7}$
7.9 – 13	$55.8^{\pm 6.3}_{\pm 12.9}$	1.93 – 2.26	$93.5^{\pm 11.2}_{\pm 17.5}$	2.90 – 3.50	$54.0^{\pm 5.9}_{\pm 8.4}$
13 – 19	$43.1^{\pm 5.5}_{\pm 9.8}$	2.26 – 2.69	$73.2^{\pm 8.1}_{\pm 13.5}$	3.50 – 4.70	$19.9^{\pm 2.5}_{\pm 3.9}$
19 – 63	$6.44^{\pm 0.74}_{\pm 1.23}$	2.69 – 3.13	$43.6^{\pm 5.4}_{\pm 10.6}$	4.70 – 8.00	$4.72^{\pm 0.72}_{\pm 0.94}$

Q^2 /GeV^2	$(d\sigma_\pi/dQ^2)^{\pm stat}_{\pm tot}$ /$\frac{\text{pb}}{\text{GeV}^2}$	Q^2 /GeV^2	$(d\sigma_\pi/dQ^2)^{\pm stat}_{\pm tot}$ /$\frac{\text{pb}}{\text{GeV}^2}$
$2.0 < Q^2 < 70.0$ GeV^2		$p^\star_{T,\pi} > 2.5$ GeV (hcms)	
2.00 – 2.40	$139^{\pm 16}_{\pm 29}$	6.50 – 9.10	$19.0^{\pm 1.8}_{\pm 3.6}$
2.40 – 3.00	$106^{\pm 11}_{\pm 23}$	9.10 – 13.0	$11.5^{\pm 1.1}_{\pm 1.8}$
3.00 – 3.80	$78.2^{\pm 7.3}_{\pm 13.3}$	13.0 – 20.0	$7.12^{\pm 0.68}_{\pm 1.23}$
3.80 – 4.90	$54.5^{\pm 4.8}_{\pm 10.5}$	20.0 – 32.0	$3.64^{\pm 0.36}_{\pm 0.63}$
4.90 – 6.50	$35.5^{\pm 3.1}_{\pm 5.3}$	32.0 – 70.0	$1.08^{\pm 0.10}_{\pm 0.22}$

$x \cdot 10^4$	$(d\sigma_\pi/dx)^{\pm stat}_{\pm tot}$ /nb	Q^2 /GeV^2	$(d\sigma_\pi/dQ^2)^{\pm stat}_{\pm tot}$ /$\frac{\text{pb}}{\text{GeV}^2}$
$2.0 < Q^2 < 70.0$ GeV^2		$p^\star_{T,\pi} > 3.5$ GeV (hcms)	
1.0 – 1.9	$374^{\pm 41}_{\pm 70}$	2.00 – 3.00	$35.0^{\pm 4.4}_{\pm 7.7}$
1.9 – 3.0	$249^{\pm 32}_{\pm 45}$	3.00 – 4.90	$22.5^{\pm 2.3}_{\pm 3.9}$
3.0 – 5.0	$165^{\pm 21}_{\pm 30}$	4.90 – 9.10	$10.0^{\pm 1.0}_{\pm 1.5}$
5.0 – 11	$60.3^{\pm 6.5}_{\pm 10.5}$	9.10 – 20.0	$3.20^{\pm 0.35}_{\pm 0.55}$
11 – 63	$5.90^{\pm 0.69}_{\pm 1.50}$	20.0 – 70.0	$0.64^{\pm 0.07}_{\pm 0.11}$

Table 1: The numerical values of the inclusive differential π°-meson cross sections as shown in Figures 1-4. The value of the cross section is presented together with the respective statistical and total error. The phase space is given by $0.1 < y < 0.6$, $5^\circ < \theta_\pi < 25^\circ$ and $x_\pi > 0.01$ in addition to the restrictions given in the Table.

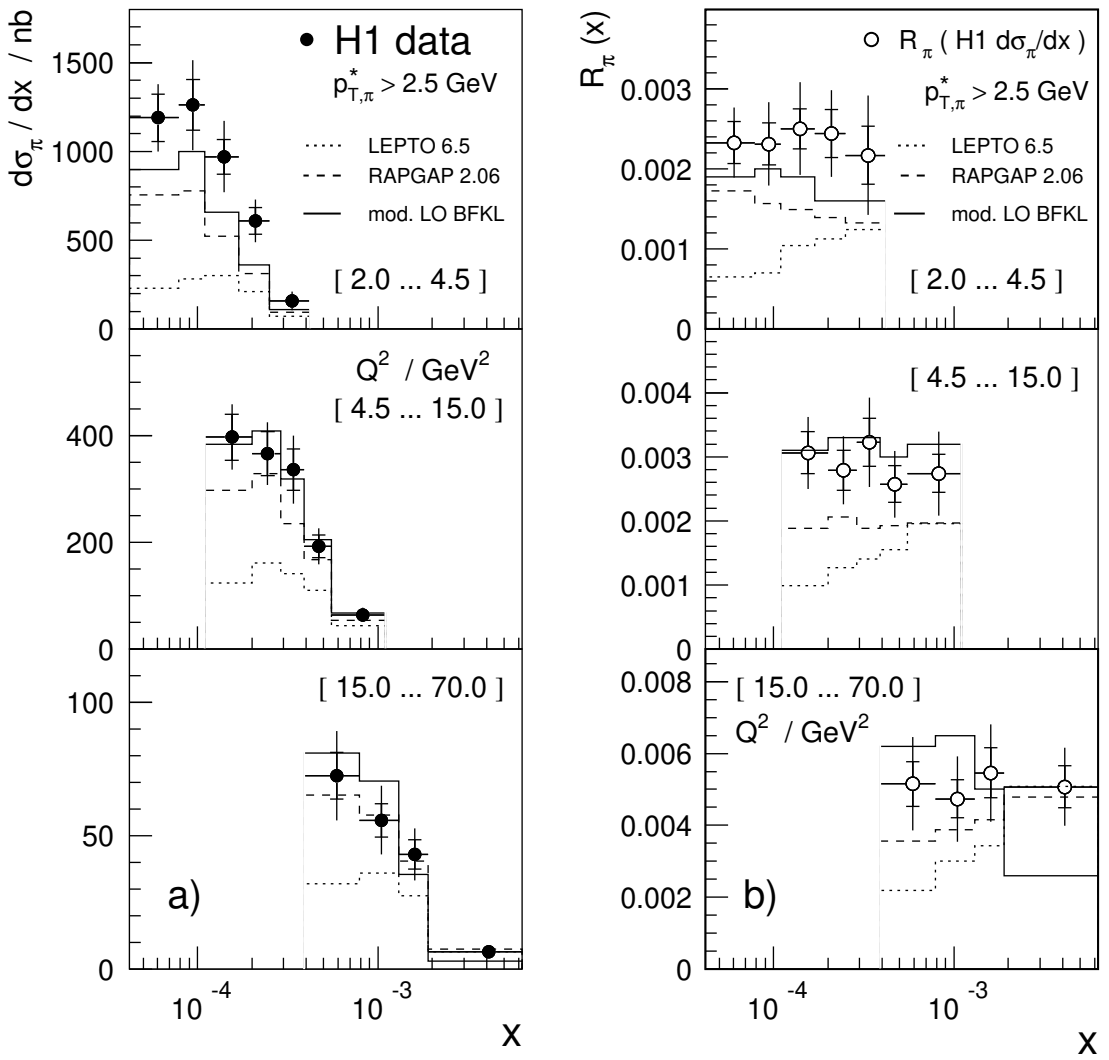

Figure 1: Inclusive π°-meson production cross-sections as a function of x for $p^\star_{T,\pi} > 2.5$ GeV in three regions of Q^2 (a). The phase space is given by $0.1 < y < 0.6$, $5^\circ < \theta_\pi < 25^\circ$ and $x_\pi = E_\pi / E_{proton} > 0.01$ and the Q^2 ranges given in the figure. The inner error bars are statistical, and the outer error bars give the statistical and systematical error added quadratically. θ_π and x_π are measured in the H1 laboratory frame, $p^\star_{T,\pi}$ is calculated in the hadronic CMS. The QCD models RAPGAP (sum of direct and resolved contributions) and LEPTO are compared to the data. Also shown is the prediction of the modified LO BFKL calculation by Kwiecinski, Martin and Outhwaite. Figure (b) shows the rate of π°-meson production in DIS as a function of x obtained by dividing the cross-section shown in (a) by the inclusive ep cross-section in each bin of x and Q^2 .

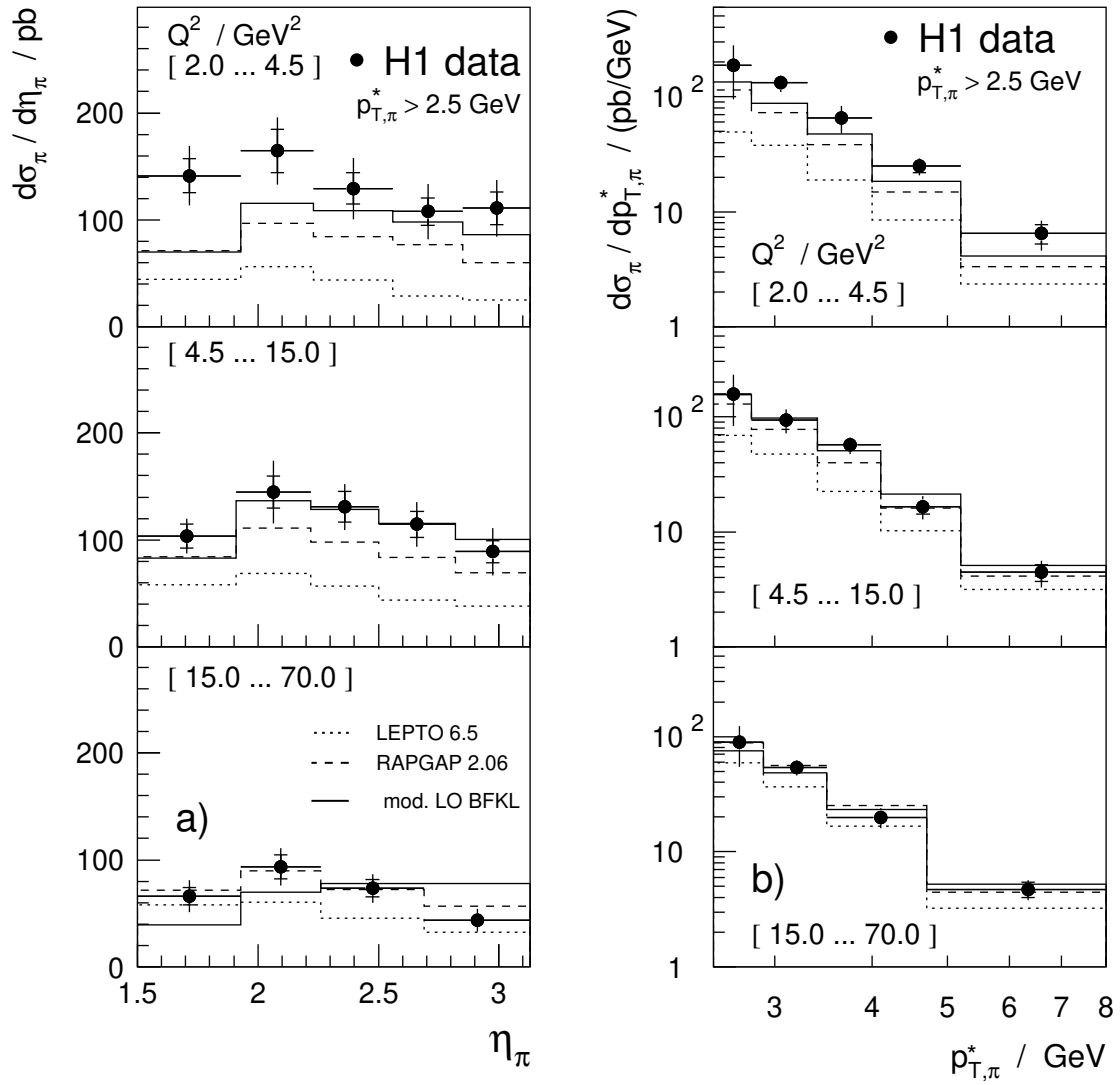

Figure 2: Inclusive π°-meson production cross-sections as a function of η_π (a) and $p^\star_{T,\pi}$ (b) for $p^\star_{T,\pi} > 2.5$ GeV in three regions of Q^2 . The phase space is given by $0.1 < y < 0.6$, $5^\circ < \theta_\pi < 25^\circ$ and $x_\pi = E_\pi / E_{proton} > 0.01$ and the Q^2 ranges given in the figure. The inner error bars are statistical, and the outer error bars give the statistical and systematical error added quadratically. θ_π and x_π are measured in the H1 laboratory frame, $p^\star_{T,\pi}$ is calculated in the hadronic CMS. The QCD models RAPGAP (sum of direct and resolved contributions) and LEPTO are compared to the data. Also shown is the prediction of the modified LO BFKL calculation by Kwiecinski, Martin and Outhwaite.

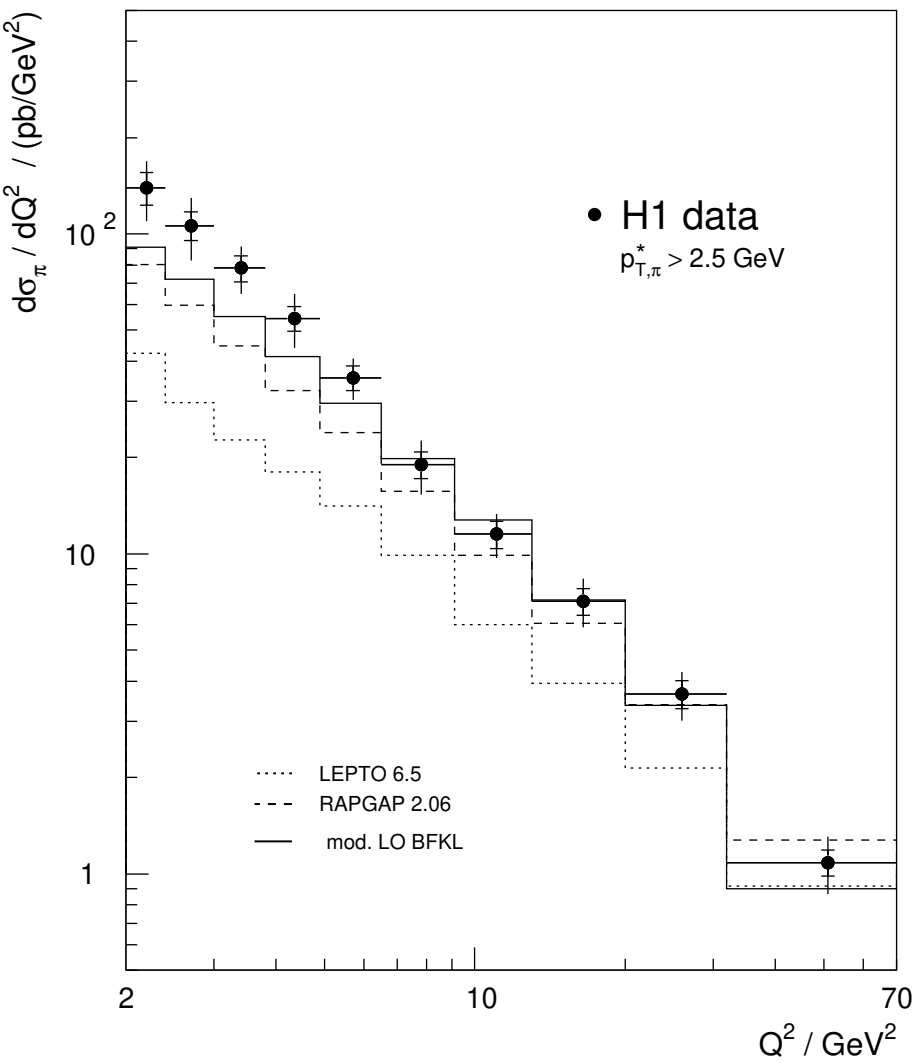

Figure 3: Inclusive π°-meson production cross-sections as a function of Q^2 for $p^\star_{T,\pi} > 2.5$ GeV. The phase space is given by $0.1 < y < 0.6$, $5^\circ < \theta_\pi < 25^\circ$ and $x_\pi = E_\pi / E_{proton} > 0.01$. The inner error bars are statistical, and the outer error bars give the statistical and systematical error added quadratically. θ_π and x_π are measured in the H1 laboratory frame, $p^\star_{T,\pi}$ is calculated in the hadronic CMS. The QCD models RAPGAP (sum of direct and resolved contribution) and LEPTO are compared to the data. Also shown is the prediction of the modified LO BFKL calculation by Kwiecinski, Martin and Outhwaite.

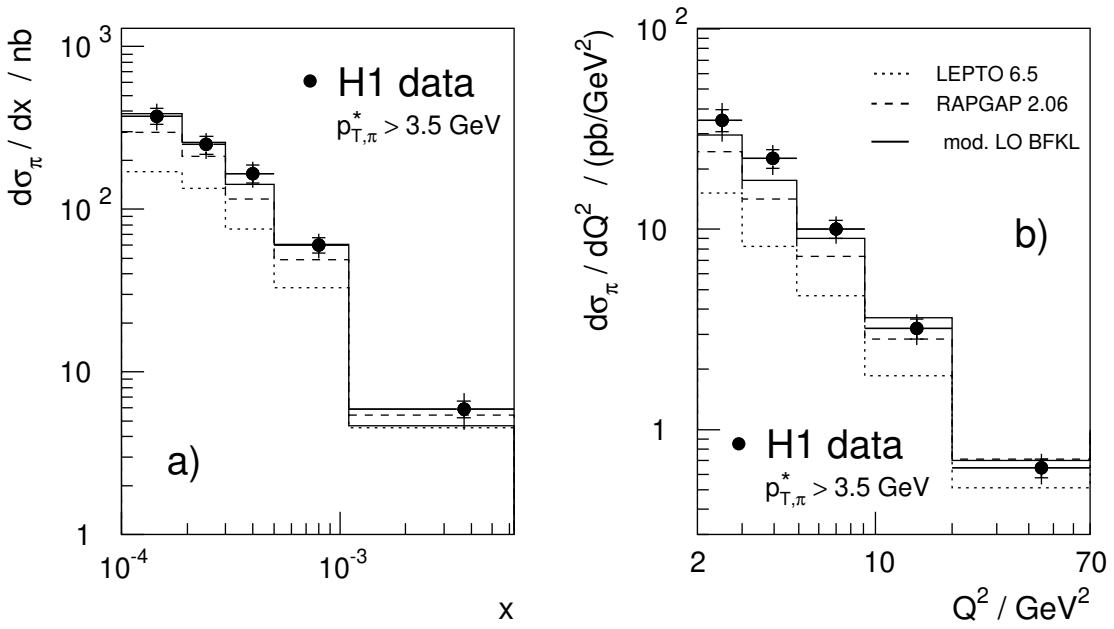

Figure 4: Inclusive π°-meson production cross-sections as a function of x (a) and Q^2 (b) for $p^{\star}_{T,\pi} > 3.5$ GeV. The phase space is given by $2.0 < Q^2 < 70.0\ \mathrm{GeV}^2$, $0.1 < y < 0.6$, $5^{\circ} < \theta_{\pi} < 25^{\circ}$ and $x_{\pi} = E_{\pi}/E_{proton} > 0.01$. The inner error bars are statistical, and the outer error bars give the statistical and systematical error added quadratically. θ_{π} and x_{π} are measured in the H1 laboratory frame, $p^{\star}_{T,\pi}$ is calculated in the hadronic CMS. The QCD models RAPGAP (sum of direct and resolved contribution) and LEPTO are compared to the data. Also shown is the prediction of the LO BFKL calculation by Kwiecinski, Martin and Outhwaite.